Surface & Coatings Technology 383 (2020) 125252

Contents lists available at ScienceDirect

Surface & Coatings Technology

journal homepage: www.elsevier.com/locate/surfcoat

How nanoparticles and submicron particles adsorb inside coating during plasma electrolytic oxidation of magnesium?

M. Asgari, M. Aliofkhazraei*, Gh. Barati Darband, A. Sabour Rouhaghdam

Department of Materials Engineering, Tarbiat Modares University, P.O. Box: 14115-143, Tehran, Iran

ARTICLE INFO

Keywords:
Alumina
Corrosion
Magnesium
Nanoparticle
Urea
Wear

ABSTRACT

The effects of seven different additives including ethanol, methanol, glycerin, triethanolamine (TEA), urea, formamide and sodium dodecyl sulfate (SDS) were investigated on the incorporation of alumina nanoparticles (NPs) and submicron particles in plasma electrolytic oxidation of AZ31B magnesium alloy substrates. Initial results from weight changes indicate that the additives did not improve the incorporation of submicron particles, whereas the incorporation of NPs was indeed enhanced. The most efficient additive was found to be urea which resulted in the highest content of alumina NPs to be incorporated. Later, the impact of urea concentration was investigated and it was discovered that the highest incorporation of NPs occurred at 20 g/l of urea concentration, in which NPs were properly dispersed into the solution and their size was decreased. Corrosion and wear properties of films which were evaluated either with or without urea were studied. The highest content of incorporated alumina NPs was obtained at 20 g/l of urea. DLS results show that 20 g/l urea caused the lowest size of particles in the electrolyte. The highest corrosion resistance (with a current density of 1.5 mA/cm^2) and the lowest wear rate (approximately 0.1 μg/N·m) were achieved at 20 g/l of urea concentration.

1. Introduction

Magnesium alloys are widely utilized in industrial applications such as automobile, aerospace, electronics, computers, cell phones, etc. due to their desirable mechanical and physical properties, and are being extensively studied by researchers around the globe [1–3]. In spite of all the favorable properties, magnesium and its alloys suffer from poor corrosion, wear and creep resistance as well as a high chemical activity which have limited their applications [4–6]. Magnesium has higher chemical activity than other prevailing metals such as aluminum, zinc, and manganese, hence its alloys exhibit lower corrosion resistance than those of the other metals. This obstacle has hampered the efforts for the usage of magnesium alloys in engineering applications [7–9].

Therefore, magnesium alloys must be protected properly. Being the most efficient approach in preventing corrosion, anti-corrosion coatings have to be developed on magnesium alloys in order to overcome the existing constraints. The commonly used techniques for fabrication of such coatings consist of conversion coating, electrodeposition, organic films, physical vapor deposition (PVD), and more recently, plasma electrolyte oxidations (PEO). PEO could be a promising method for the protection of magnesium alloys due to low costs and simplicity of process as well as providing relatively high corrosion and wear resistance [10,11].

The main advantage of PEO films is the improvement of several qualities such as corrosion resistance, wear resistance, surface morphology and etc. However, in corrosion applications, PEO films are susceptible to destruction due to porous morphology and permeability in such environments. The corrosion resistance of PEO films may be further improved through adjustment of the electrolyte chemical composition, process indices and sealing of the active sites such as pores and cracks on the surface [12–14].

Films with higher hardness, wear and corrosion resistance than typical magnesium alloys are obtained via the PEO process. However, such films are porous and cannot act as an indestructible barrier for long-term protection purposes; therefore, both avoiding the formation of a highly porous film and sealing the produced film are essential. The chemical composition of electrolyte is considered as a significant parameter in the properties of the produced films [15]. An electrolyte with a certain chemical composition is usually employed in the PEO process while different properties such as wear and corrosion resistance as well as hardness may be altered by the introduction of particles to the electrolyte, formation of various phases or incorporation of particles within the films. One may predict the role of any sort of particle according to its melting point, chemical stability, type of bonds and size [16,17].

Nanostructured films have attracted a great deal of attention over the past few years as they are capable of fabricating materials with

* Corresponding author.
E-mail addresses: maliofkh@gmail.com, khazraei@modares.ac.ir (M. Aliofkhazraei).

https://doi.org/10.1016/j.surfcoat.2019.125252
Received 27 September 2019; Received in revised form 8 December 2019; Accepted 10 December 2019
Available online 12 December 2019

Table 1
Summarize of researches in the field of PEO nanocomposite coating on magnesium.

Micro/nano-particle	Type of particles	Size of particles	Incorporation of particles (wt%)	Preparation of suspension	Effect on properties of PEO coatings	Ref
Nanoparticles	Clay	50	Si = 10	Stirrer (high speed)	More closed porosity is visible	[35]
	Silica	12	9	A stirrer and bubbling with compressed air	Reactively incorporated	[36]
	HA	100	< 12	stirrer	More abundant and penetrate deeper in the coating	[37]
	Alumina	30	< 10	Dispersed evenly in the solution	Improved thickness, hardness and corrosion resistance.	[38]
	Zirconia	100	1.7	Surfactant	Improved corrosion and wear resistance	[17]
	Silica	100	8	surfactant	Improved corrosion and wear resistance	[17]
Micro-particles	Silica	1–5 μm	5	A stirrer and bubbling with compressed air	Inertly incorporated	[36]
	HA	2.5 μm	< 5	Powders were slowly added under vigorous stirring	Not penetrate	[37]
	Ceria	5	2	Stirrer (high speed)	Corrosion resistance was increased	[39]

unique chemical and physical properties [18]. Grain refinement is a practical method of achieving higher degrees of hardness and strength in a metallic bulk. This also applies to coatings where superior mechanical properties may be acquired through refinement. Proper mechanical and chemical properties of a nanocomposite film hinge on high hardness, toughness, adhesion strength and chemical and thermal stability and low friction [19]. Gnedenkov et al. [20] fabricated the coatings on the surface of magnesium alloy by PEO with ZrO_2 and SiO_2 NPs. They discovered that the addition of these NPs to PEO coating can enhance the properties significantly [20]. The results indicate that zirconia exhibited a better influence on corrosion and mechanical properties. They reported that polarization resistance of coating with zirconia is twice as high as the PEO coating without NPs and that the wear rate of coating is lowered by half. Many researchers have reported an improvement in corrosion and wear resistance by the addition of Al_2O_3 NPs [21]. The effect of Al_2O_3 NPs on corrosion resistance and hardness of films has been studied by Wang et al. [22]. It was reported that particle dispersion in the suspension was highly effective in the quality of films. The mechanical properties of nanocomposite films reinforced with alumina NPs which were produced by means of micro-arc oxidation technique on titanium substrates were studied [14]. With regards to the surface roughness of the films, it has been reported that NPs filled the volcano-like valleys on the surfaces so that the difference between high and low areas was diminished, hence it was observed that surface roughness decreased with an increase in NPs concentration as well as in coating duration. It was also mentioned that hardness was improved when a higher concentration of NPs was added into the electrolyte. Wear resistance also appeared to be enhanced with increase in concentration of NPs. According to the investigations carried out on the worn areas following the wear test, it was stated that the partially worn areas had a proper distribution of alumina NPs. The separated areas were also found with agglomerated NPs. The effect of Al_2O_3 NPs on corrosion resistance and hardness of films was studied by Wang et al. [22]. It was reported that particle dispersion in the suspension was highly effective in the quality of films. Sarbishei et al. investigated the effect of concentration of Al_2O_3 NPs on Ti substrate. They used 0, 3, 6, 10 g/l Al_2O_3 NPs in electrolyte and reported that sample with 10 g/l NP had the optimal corrosion resistance and the lowest porosity. It was also reported that with the increase of NPs in the electrolyte, corrosion resistance was increased from 2.3×10^4 to $1.2 \times 10^6\ \Omega{\cdot}cm^2$ [23].

Electrolyte chemical composition is a noteworthy and important factor in the structure and properties of nanocomposite films [24]. Hence, changing the chemical composition of the electrolyte can be a suitable approach in the production of films with desirable properties. Yeh et al. [25] investigated the effect of urea on the PEO process and found that the addition of urea not only increased the nitrogen content in the films but also reduced its thickness and increased precipitants in the electrolyte. However, they did not measure its effect on the incorporation of NPs. Pan et al. [26] studied the effect of several additives including glycerin on the PEO process. It was reported that electrolyte conductivity, film thickness, and oxygen evolution were reduced with the addition of glycerin in an ammonium bifluoride electrolyte. On the other hand, arc size, electrolyte temperature, and film adhesion were increased in the presence of glycerin. Gnedenkov et al. [17] studied the nanocomposite films containing silica and zirconia NPs and used SDS for dispersion of particles inside the solution. It was established that SDS kept the solution stable. This suspension was dispersed through ultrasonication. Elsewhere, SDS was used by Vasilyeva et al. [27] for the dispersion of manganese oxide and nickel oxide particles in an electrolyte. Sarbishei et al. [28] applied TEA as a surfactant for alumina NPs. Furthermore, it was confirmed that alumina NPs were not properly incorporated without surfactant and additive [14], hence, the use of TEA was necessary. Li et al. [29,30] used formamide and TEA in two studies to adjust the electrical conductivity of the solution. They concluded that coating in the electrolyte containing formamide and TEA resulted in the formation of a thick film on titanium. Kim et al. [31]

reported that the addition of ethanol to a solution containing hydroxyapatite particles reduced gas evolution during the process, and also facilitated the incorporation of HA particles on the porous surface. Mu et al. [32] investigated self-lubricant titania graphite films. According to their results, ethanol should be present in the electrolyte in order to make sure of the wetting and the dispersion of graphite particles. There has been a great deal of debate in this matter; however, it may be concluded that various additives change the surface of particles so that NPs may be better incorporated [33,34].

The majority of published papers in related field have investigated several parameters such as the effect of various nanoparticles and micro-particles, the effect of concentration of particles, etc. (Table 1). The main goal in this work is to enhance the incorporation of alumina NPs (of various sizes) by means of the introduction of different organic additives. It should be noted that all of these additives are organic, readily accessible and inexpensive so that they might be easily acquired and tested.

2. Experimental procedure

PEO method was employed in order to deposit oxide films on AZ31B magnesium alloys. Samples were cut to pieces with dimensions of $4 \times 2.5 \times 0.2\,cm^3$. Through the preparation process, samples were initially polished with 400# to 1500# sandpapers and then degreased in an alcohol solution. Chemical analysis of AZ31B magnesium alloys is presented in Table 2. The deposition current was DC and AISI 304 stainless steel was used as cathode which came in the shape of a rectangular plate with dimensions of $50 \times 80\,mm^2$. A 20 kW rectifier was used for the deposition process. Dilute alkaline solutions containing alumina micro- and NPs (Particles with two different size ranges (nano-scale around 40 nm and sub-micron scale around 300 nm)) were added in the process. TEM images of NPs were taken by a JEOL-2010 TEM (Fig. 1). The utilized electrolyte contained 5 g/l of sodium phosphate, 30 g/l of potassium hydroxide (both manufactured by MERCK Inc. with analytical purity) and 30 g/l of alumina NPs. A constant pH was fixed at 12–12.5 for all solutions. In order to uniformly disperse NPs in the solution, they were mixed twice in distilled water for 24 h on a stirrer. Each solution was stirred via ultrasonic for 30 min prior to the process. In order to achieve a precise rotation rate, a mechanical stirrer was employed. The optimized deposition conditions in the present work included the current density of $100\,mA/cm^2$ and electrolyte rotation rate of 100 rpm [40]. The duration of the PEO coating was kept at 5 min. Lengthier PEO durations incurred damage to the sample by causing sizeable sparks. Seven additives (methanol (5 g/l), ethanol (5 g/l), formamide (5 g/l), TEA (5 g/l), urea (0–20 g/l), SDS (5 g/l) and glycerin (5 g/l)) were applied in this process. The effect of each additive on the incorporation of alumina NPs was investigated. Weight changes in samples were measured by a high-precision micro-balance (± 50 μg). For evaluating the voltage-time response of the coating system, a voltmeter with a precision of 1 mV (fluke 289) was connected to the setup. The positive pole was connected to anode (sample) while the negative pole was attached to cathode (rectangular stainless steels). Then, the voltmeter connected to a computer device with USB and the relevant software recorded variation of voltage with time. The structure of films was studied by SEM images obtained with XL30 Philips Scanning electron microscope (SEM). In addition, the porosity of the samples was obtained by means of image processing with image j software. The average size of Al_2O_3 NPs in the PEO suspensions with 30 g/l concentration of alumina was determined using a DLS spectroscopy (model; Zetasizer NanoZS). The corrosion resistance of films was evaluated in conventional 3.5 wt% NaCl with a pH of 7.9. Prior to electrochemical tests, samples were exposed to the corrosive solution for 15 min to reach stable potential. PDP (according to ASTM G5) and EIS (according to ASTM G106) tests were carried out for investigation of corrosion behavior. EG&G (model 273A equipped with FRA system) potentiostat/galvanostat was used for electrochemical tests. These tests were conducted in a (a) standard electrochemical cell with three electrodes. Pt, saturated calomel electrode (SCE) and the main sample were used as the counter electrode, reference electrode, and working electrode respectively. The scanning rate was 1 mV/s in the PDP test which started from −0.2 V vs. OCP and continued up to +0.8 V vs. SCE. The EIS frequency range was from 65.5 kHz to 10mHz with the amplitude of 10 mV around open circuit potential (OCP). Wear resistance was studied by pin-on-disk wear test (according to ASTM G99-17). A polymer-based composite pin made from POLYBON (a polymer-based composite substance) was used as the counter-abrading material. The applied load and rotation rate were 45 N and 100 rpm, respectively. The wear track with a length of 200 m was kept similar for all samples. Hardness test was conducted using microhardness tester with a Vickers indenter under a load of 15 g and a loading duration of 10 s.

Table 2
Chemical composition of the alloy used for deposition.

Element	Fe	Si	Ni	Mn	Cu	Zn	Al	Mg
%wt	0.001	0.01	0.002	0.64	0.01	0.9	3.5	Balance

3. Results and discussion

3.1. Effects of different additives

There are various parameters affecting the incorporation of particles, such as particle size and the type of additives used in the electrolyte. After the dispersion of particles in the electrolyte and mixture with hydroxide ions, particles are negatively charged. Due to the strong electrical field between anode and cathode, the charged particles are pushed towards the positive electrode (anode) [41,42]. It should be mentioned that NPs normally tend to agglomerate, and consequently, form sediments on the bottom of the container. Hence, through various techniques, particles have to be kept uniformly dispersed in the solution [23,28]. Although other parameters such as electrolyte stirring rate, the concentration of NPs, current density and deposition time have been previously investigated, the effects of additives and particle size have yet to be studied [40]. Additives can improve both dispersion and incorporation of NPs by modifying particle surfaces. The effects of additives and the size of alumina NPs on the incorporation of the particles are shown in Fig. 2a and b. As other variables were kept constant, weight changes of films can be attributed merely to variations in the incorporation of particles. It was mentioned earlier that seven organic materials (methanol, ethanol, formamide, TEA, urea, SDS and glycerin) were used. Particles with two different size-range (nano-scale around 40 nm and sub-micron scale around 300 nm) were investigated. The effects of additives on the incorporation of NPs are illustrated in Fig. 2a. It can be observed that urea has resulted in the highest degree of incorporation compared to others. Glycerin, methanol, TEA, formamide and ethanol were the next additives that increased enhanced the incorporation of NPs.

Fig. 2b shows the effects of additives on the incorporation of submicron-sized particles. Accordingly, SDS resulted in the highest amount of the incorporated submicron particles while formamide, glycerin, TEA, methanol, ethanol, and urea were rated next. However, it is clear that none of the additives could impose a significant change in the incorporation of microparticles. This is probably due to the fact that these particles were too large to be affected by any sort of additive [43].

Chemical composition of the electrolyte and particularly the presence of different types of particles in the electrolyte, which has to be followed by their incorporation into the film, has a great impact on morphology and porosity of the produced films [44]. SEM image of the surfaces and cross-sections of coated samples in solutions containing different types of additives and particles of nano-scale and submicron sizes are illustrated in Figs. 3 and 4, respectively. Fig. 3 shows the

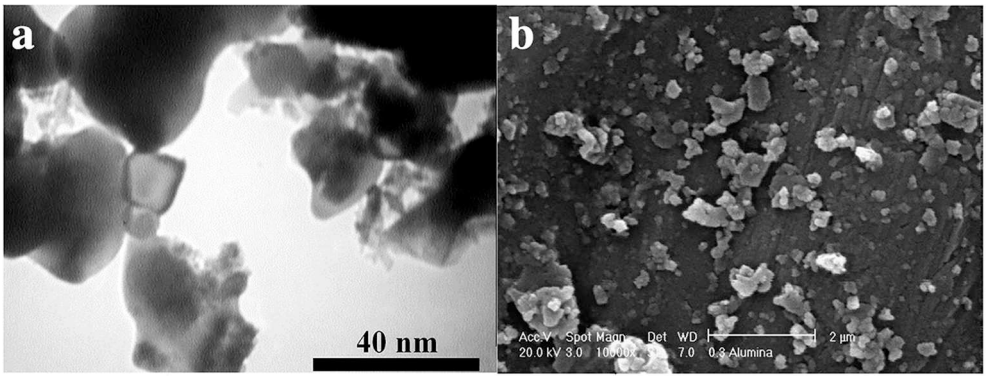

Fig. 1. TEM image (bright field) of alumina NPs (with the average size of 30 nm).

surface morphology of films coated in the electrolyte containing alumina NPs and various other additives. It is observed that the presence of NPs changed the surface structure and that their incorporation has been facilitated by additives. The preferred incorporation sites were mostly located at the center of volcano-like pores [45]. Several of the existing pores were filled with NPs. Mirzamohammadi et al. [46] studied the effect of organic additives on the incorporation of NPs in the electroplating process and reported that particles became hydrated while they were dispersed in the electrolyte. A gap was formed between the particles and the electrode after the hydration process. It was mentioned that the thickness of the hydrate film depended on several parameters such as NP type, electrolyte chemical composition, and additive type. As the first two parameters were constant, it could be derived that solely the effects of additives were investigated. The thinner hydrate layer caused the particles to be placed closer to the electrode and increased the chance of their eventual incorporation. Thiemig et al. [47] reported that the presence of ethanol in Watt's bath had a noticeable effect on thickness of the hydrate layer. They worked on electrodeposition of nanocomposites through electroplating and witnessed that NPs drew nearer to the electrode as the thickness of the hydrate layer decreased. Gul et al. [48] reported that a thick hydrate layer not only reduced the probability of incorporation of NPs but also increased number of elastic collisions, thus reducing the incorporation of NPs. It may be concluded that presence of additives leads to the formation of a thinner hydrate layer and greater incorporation of NPs. The highest increase in incorporation of NPs was observed in the sample coated in electrolyte which contained urea with nano-scale particles. The same cannot be said about submicron particles, since they are both larger and heavier than NPs. Consequently, they cannot get wet easily and they also tend to sediment more quickly. They are not light enough to be neglected. These are the causes for the incorporation of micro-particles being lower than that of the NPs [49]. Gue et al. [50,51] investigated PEO composite coatings and stated that in addition to stabilizing the solution through improving the wettability of its particles, surfactants also contributed towards an increase in electrostatic incorporation of the suspended particles on the anode by means of creating a net positive charge. According to them, anion surfactants increased the negativity of PTFE NPs and, lead to the improvement of electrophoretic bonds which caused electrostatic incorporation of NPs on the magnesium anode in the PEO process.

SEM images of surfaces and cross-sections of films coated in the electrolyte containing microparticles and different types of additives are presented in Fig. 4. It may be deducted that no additive could be significantly effective in the incorporation of submicron-sized particles. In fact, the degree of incorporation plummeted proportionally with increased particle size. According to the cross-sections images, there is an acceptable adhesion between the film and substrate and no voids can be observed there.

Variations in the thickness of films produced in the presence of different types of additives are plotted in Fig. 5a. The thinnest film was obtained when urea was added. Thickness tended to increase further with the addition of TEA, formamide, ethanol, methanol, glycerin, and SDS, respectively. Considering the fact that a decrease in thickness was accompanied by an increase in weight (Fig. 2a), it may be deduced that urea formed a film with the highest structural density. This was also confirmed by the porosity measurements illustrated in Fig. 5b.

So far, it may be stated that the highest amount of incorporation and structural density were obtained through the addition of urea and incorporation of alumina NPs. On the other hand, the addition of other additives or submicron-sized particles could not bear any considerable results. Now, it is time to achieve the optimum concentration of urea as it is certainly a vital parameter.

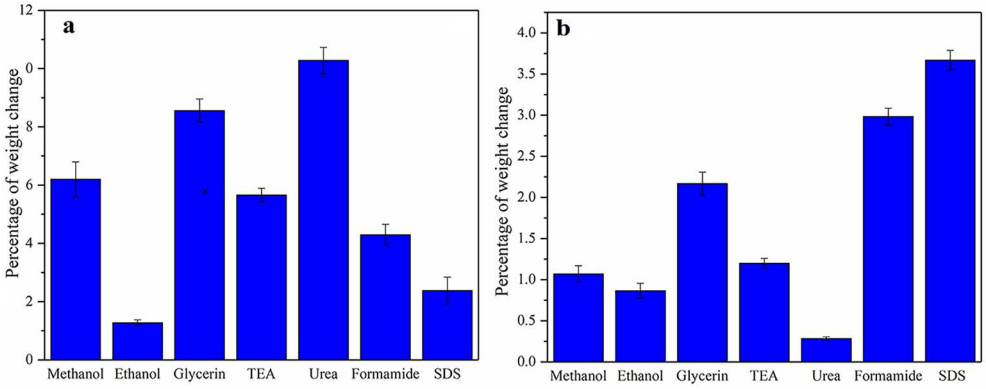

Fig. 2. The effects of various additives on incorporation of alumina, a) NPs and b) sub-micron particles.

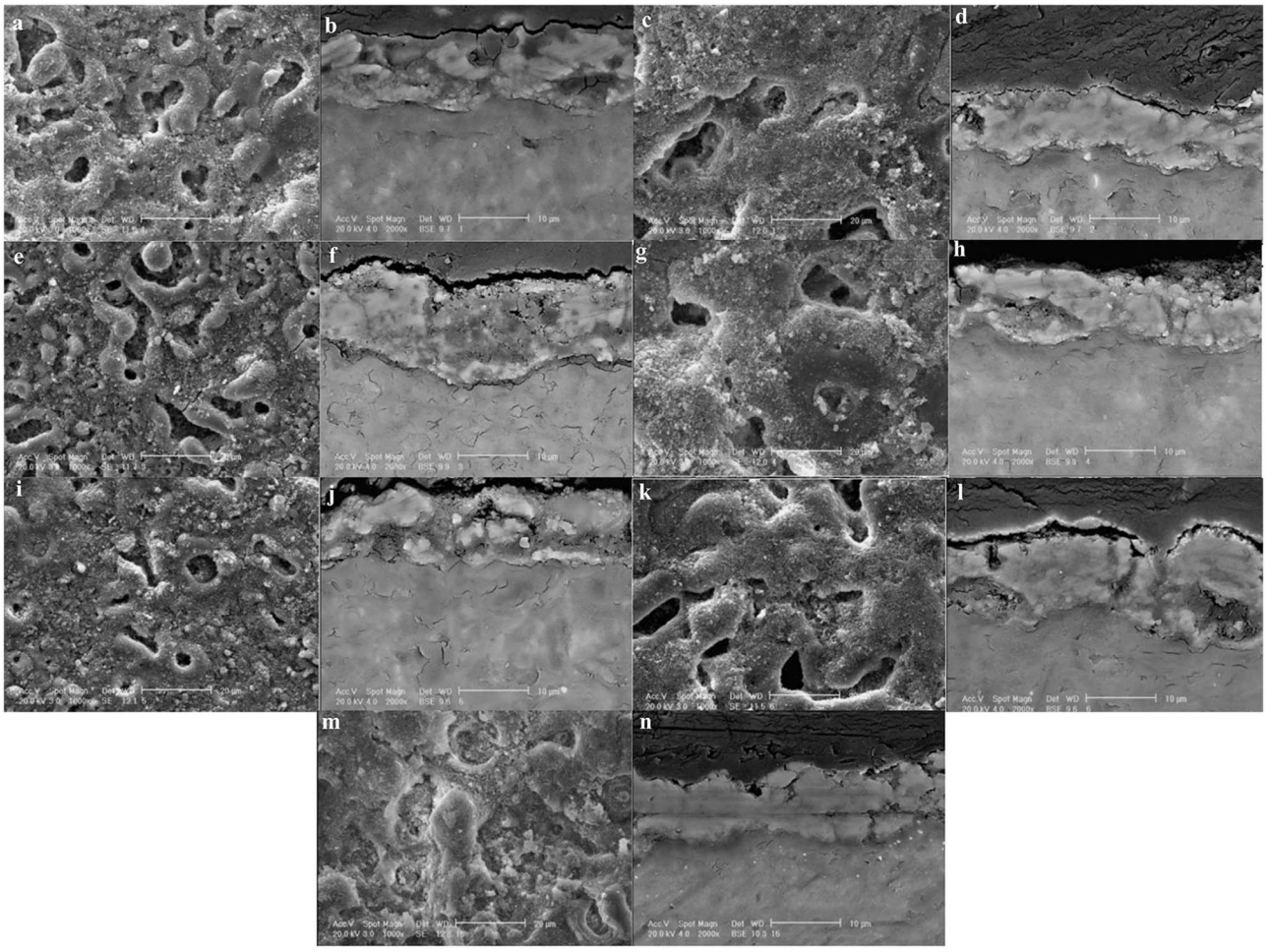

Fig. 3. SEM image of surfaces and cross sections of samples deposited in presence of NPs and a, b) methanol, c, d) ethanol, e, f) glycerin, g, h) TEA, i, j) urea, k, l) formamide, m, n) SDS.

3.2. Effect of urea

3.2.1. Surface morphology and incorporation rate of NPs

Fig. 6 shows the amount of incorporation versus the concentration of urea in the electrolyte. As it can be observed, the amount of incorporated NPs is increased proportionally with urea concentration in the electrolyte up to 20 g/l. Further increase beyond 20 g/l, however, interrupted the PEO process. In order to confirm the result extracted from weight change experiments, the EDS test results are illustrated in Fig. 6. In the EDS results, the Al element which indicted the presence of Alumina NPs in coating has been analyzed. The result of EDS and weight change measurements indicate that with the increase of urea concentration, incorporation of Alumina NPs is increased. A figure of EDS and map analyses will be discussed later. Generally, additives may have two types of influences on electrolyte: 1) they can affect the surface of the coated film [25,52]. And 2) they can act as a surfactant, improving the incorporation of NPs [53,54]. Urea exhibited the best performance in solutions with NPs which can be demonstrated based on two theories: first, it acted as a surfactant [53,54]. According to Sharifi et al. [33], atenolol was employed as a surfactant to improve the incorporation of alumina NPs in PEO films. Second, urea affected structural morphology which was investigated by Chang et al. [25]. They reported that increase in urea content resulted in an increase in surface porosity. Additionally, nitrogen content naturally rises in the presence of nitrogen-bearing additives, so that surface pores are created when gas molecules are leaving the molten oxide. It is universally accepted that NPs are preferably incorporated on high-energy sites located on the surface [13], so it may be deduced that an increase in the number of porosities may enhance the incorporation of NPs.

In order to study the effect of urea on the morphology of films, SEM images of samples coated under different urea concentrations are shown in Fig. 7. It can be observed that urea changed the surface structure and that pores were filled. According to the image of the cross-section, there exists a good adhesion between the film and the substrate. The effect of urea on the stability of the suspension is presented in Fig. 8a. It was observed that all NPs precipitated after 10 days in the electrolyte free of urea.

On the other hand, the addition of urea led to the improvement of stability in the suspension. Fig. 8b demonstrates a schematic of the sedimentation test. It can be observed that NPs sediment over time. Dynamic light scattering (DLS) test was conducted under five different urea concentrations in order to study the effect of urea on the incorporation of alumina NPs (Fig. 9a). It was observed that the addition of urea to the suspension reduced the average concentration of alumina NPs, and caused higher a greater degree of incorporation [33]. In addition, the effect of urea and the increase in its concentration on thickness and porosity of films is illustrated in Fig. 9b. Both factors appeared to be decreased with reverse proportion to urea concentration in the electrolyte.

For a precise investigation of the effect of urea in coating formation and potential – time curve of the solution is shown in Fig. 9c. Urea addition shifted potential versus time curve towards lower values. Arc voltage is clearly diminished which may be due to an increase in conductivity by the presence of urea in the electrolyte. Four successive

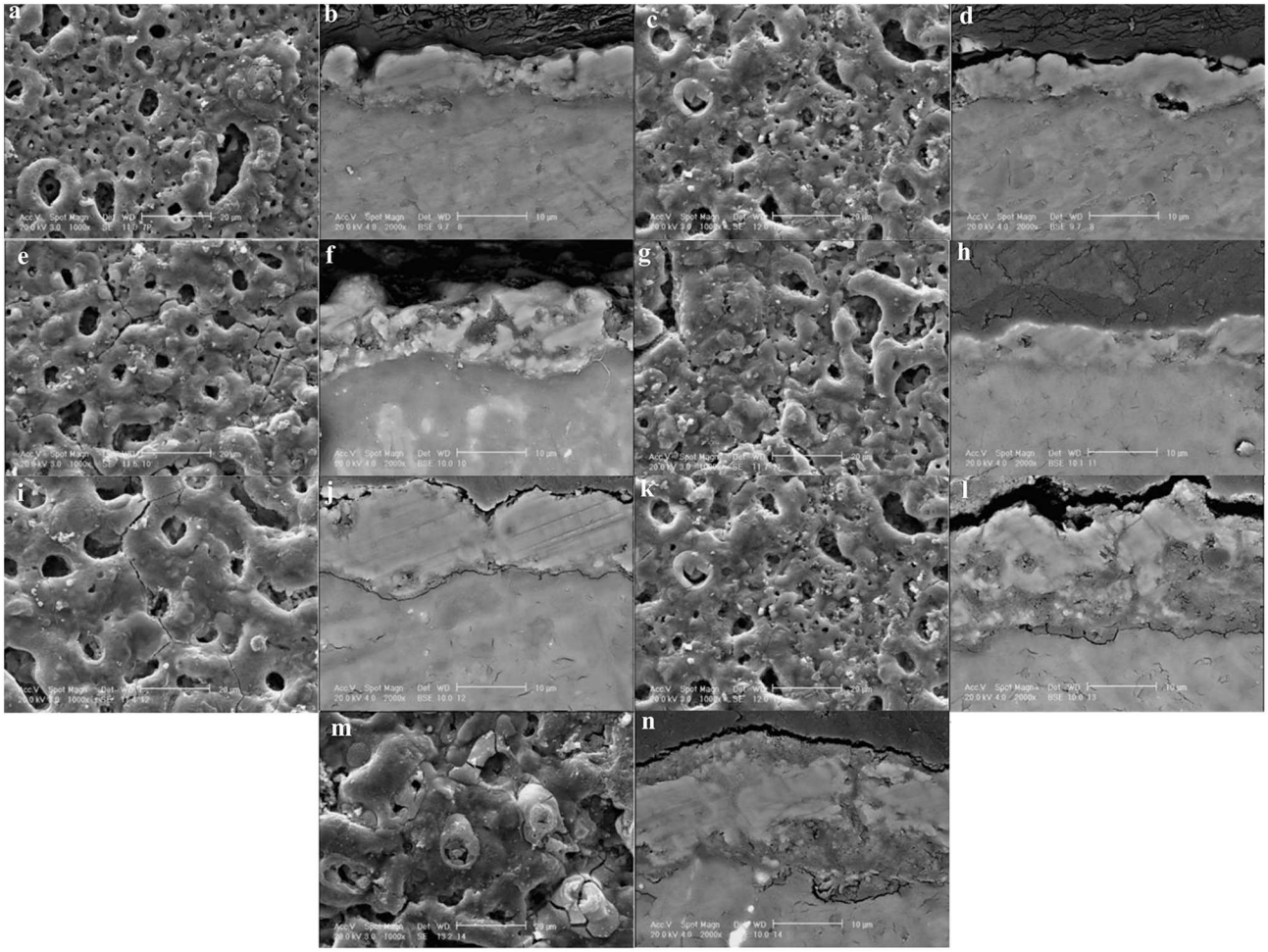

Fig. 4. SEM images of surfaces and cross sections of samples deposited in presence of micro-particles and a, b) methanol c, d) ethanol e, f) glycerin g, h) TEA i, j) urea k, l) formamide m, n) SDS.

stages are partially differentiable by voltage and surface morphology variations throughout the process. Depending on the parameters of the process, the extent of these stages is varied.

The first stage is ascribed to common anodic oxidation. Throughout this stage, voltage is increased linearly. At the end of the first stage, tiny fast-moving sparks sweep the surface [55]. Studying of electron microscope micrographs revealed that an extremely thin layer is nucleated on the surface and numerous small pores, with an opening diameter of < 100 nm, are spread all over the surface. The surface morphology in this stage is similar to that of the one created by the conventional anodizing method. It is worth noting that at this stage, the coating surface is not yet affected uniformly in its entirety [56]. During the second stage, the voltage change rate shows a decline and the curve follows a nonlinear trend. Gradually, the voltage rises and micro-arcs become slightly larger than those of the primary ones while their density is reduced. The observations conducted on the sample surface indicate that the changes in color and the roughness of the surface are boosted [57]. The coating has far fewer pores and porosities, while these pores are larger in size in comparison to the early stages. Frozen craters imply the presence of discharge channels on the surface of the coating. By increasing the voltage, the process enters the third stage, where the curve has an almost linear trend. Increasing the rate of voltage and

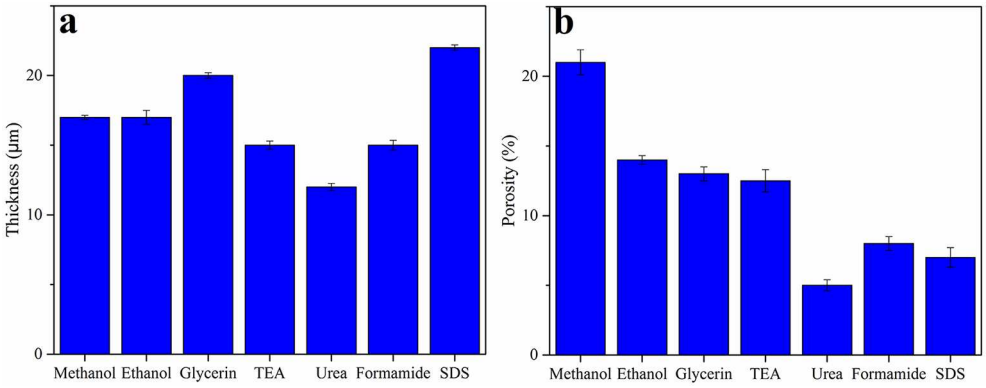

Fig. 5. Effects of additives of methanol, ethanol, glycerin, TEA, urea, formamide, SDS and NPs on a) thickness and b) porosity of films.

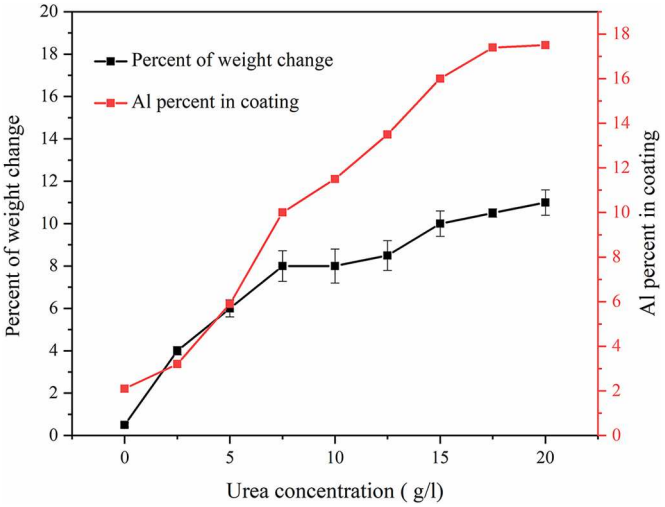

Fig. 6. Variation of incorporation rate of alumina NPs versus urea concentration.

monitoring the changes revealed that the density of micro sparks is reduced, and that the tiny sparks join and form larger sparks. In general, sparks are more sluggish than the initial state and move more slowly over the surface. The area of each micro-discharge and pore diameter is enlarged compared to second stage, and the surface roughness is increased. Studying micrographs revealed that surface of the samples is completely covered with craters that have grown in size after this phase [58]. After this stage, by further increase in voltage, the process enters the fourth stage. In this step, voltage is linearly changed with time again. No significant change is noticed in the curve slope during the coating period. Observations denote a sharp drop in the number of sparks while continue growing larger. The process is completed at this stage and the coating damage occurs. Furthermore, gas emissions from the coating surface are also declined, as they appear only at spark ignition sites. In this stage, craters continue to grow and their density is decreased. In other words, the number of sparks and their dimensions becomes smaller and larger, respectively. Due to the excessively high number of melting and re-freezing oxide coating up to this time, most craters are turned off and blocked by the neighboring volcanos [59].

Considering the conductivity measurements, it can be observed that the conductivity of the electrolyte is increased from 9.15 mS/cm in the sample without urea to 10.47 mS/cm in the sample with 20 g/l Urea. The results of conductivity tests are in good accordance with the potential-time plots.

In order to study the chemical composition of coatings, the EDS analysis of coating with NPs is shown in Fig. 10. It is clearly observed that in the coating, the main elements in coatings are Mg, O, P and Al. these elements originate from compounds that are formed during PEO coating treatment. Magnesium originates from the substrate, whereas both oxygen and phosphorus are originated from the electrolyte, and according to the elemental mapping, all elements are homogeneously

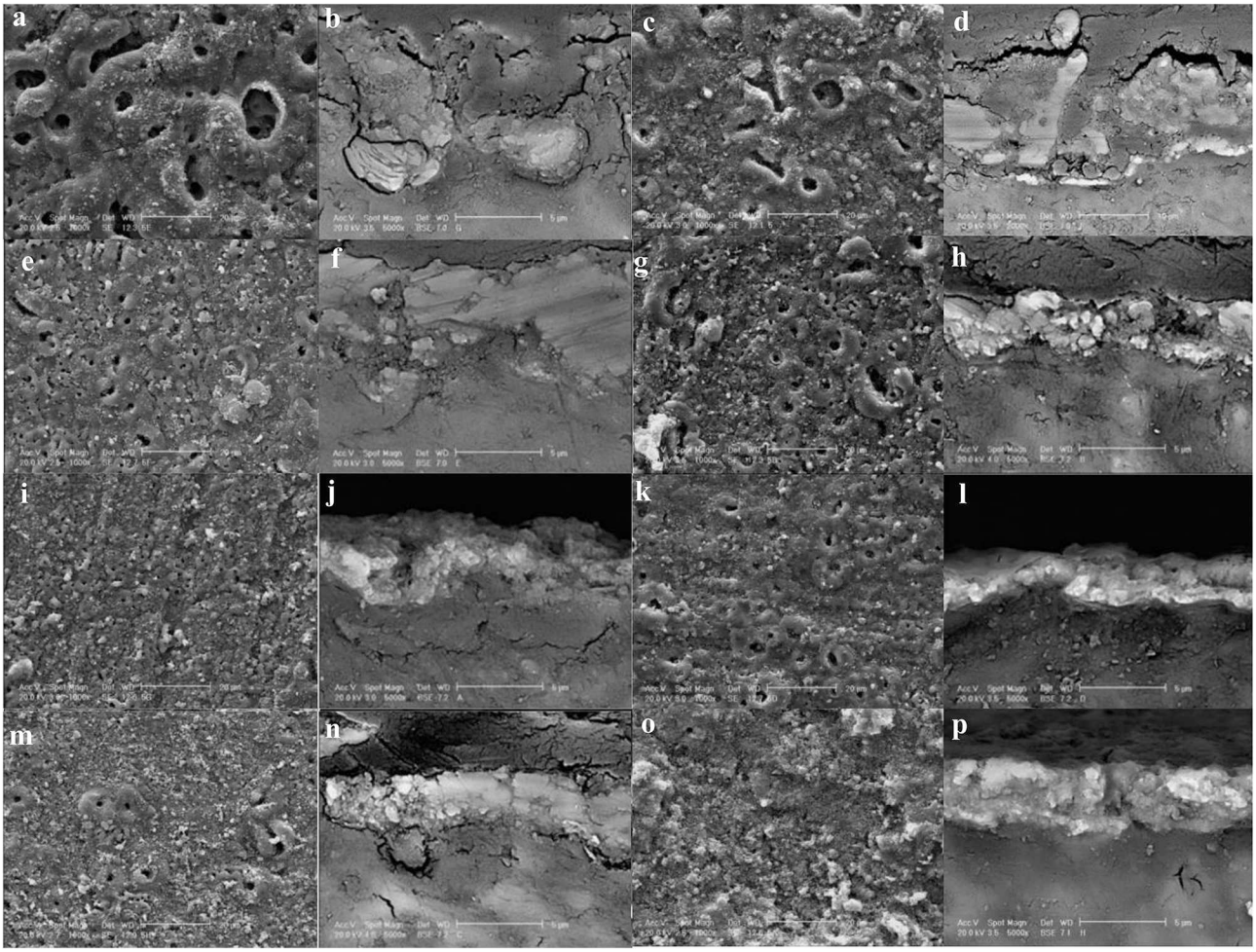

Fig. 7. SEM image of surfaces and cross sections of samples deposited in a, b) 2.5 g/l, c, d) 5 g/l, e, f) 7.5 g/l, g, h) 10 g/l, i, j) 12.5 g/l, k, l) 15 g/l, m, n) 17.5 g/l, o, p) 20 g/l concentrations of urea.

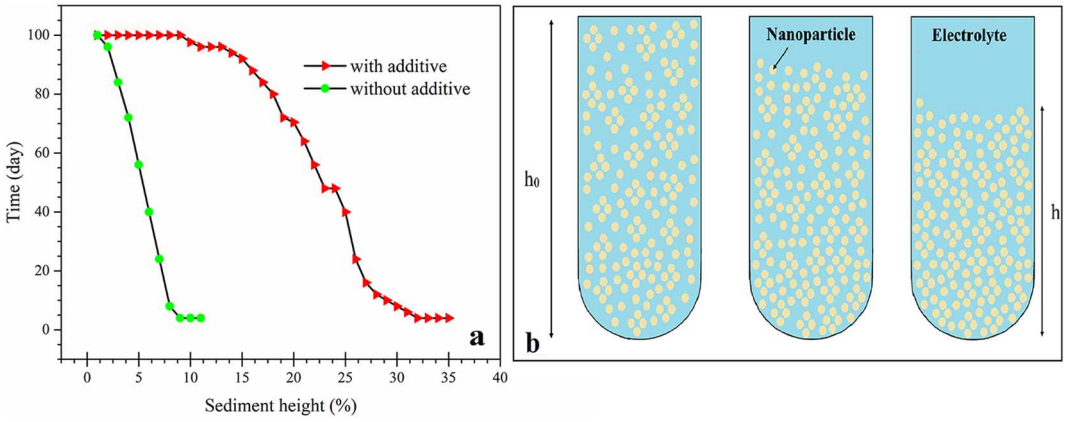

Fig. 8. a) Variation of percent of sediment height with passing time; b) a schematic figure of the precipitation test.

distributed across the coating. The presence of Al, which originates from alumina NPs, is also noted in the elemental mapping, which indicates the incorporation of alumina NPs from the electrolyte into the coating.

Furthermore, a linear scan of Al is shown at the coating cross-section in Fig. 11 which indicates an area with the highest concentration of Al in the coating's surface. Aluminum concentration is decreased by moving towards the substrate. Moreover, it can be observed from the linear scan of aluminum at coating's cross-section that the concentration of the Al element is reduced with a gentle slope towards the substrate, which indicates micro-pores being filled by alumina. Filling of micro-pores has an enormous effect on the properties of the coating such as corrosion resistance which will be discussed in the following. In the previous article, it was proven that adding alumina NPs to electrolyte resulted in the creation of alumina, phosphate, magnesia phases in the coating as evident in XRD results.

3.2.2. Corrosion behavior

3.2.2.1. Potentiodynamic polarization. The highest incorporation of NPs was achieved in the presence of urea, and corrosion resistance studies were performed using the optimum concentration of urea (20 g/l). The corrosion resistance of coatings was compared with other samples

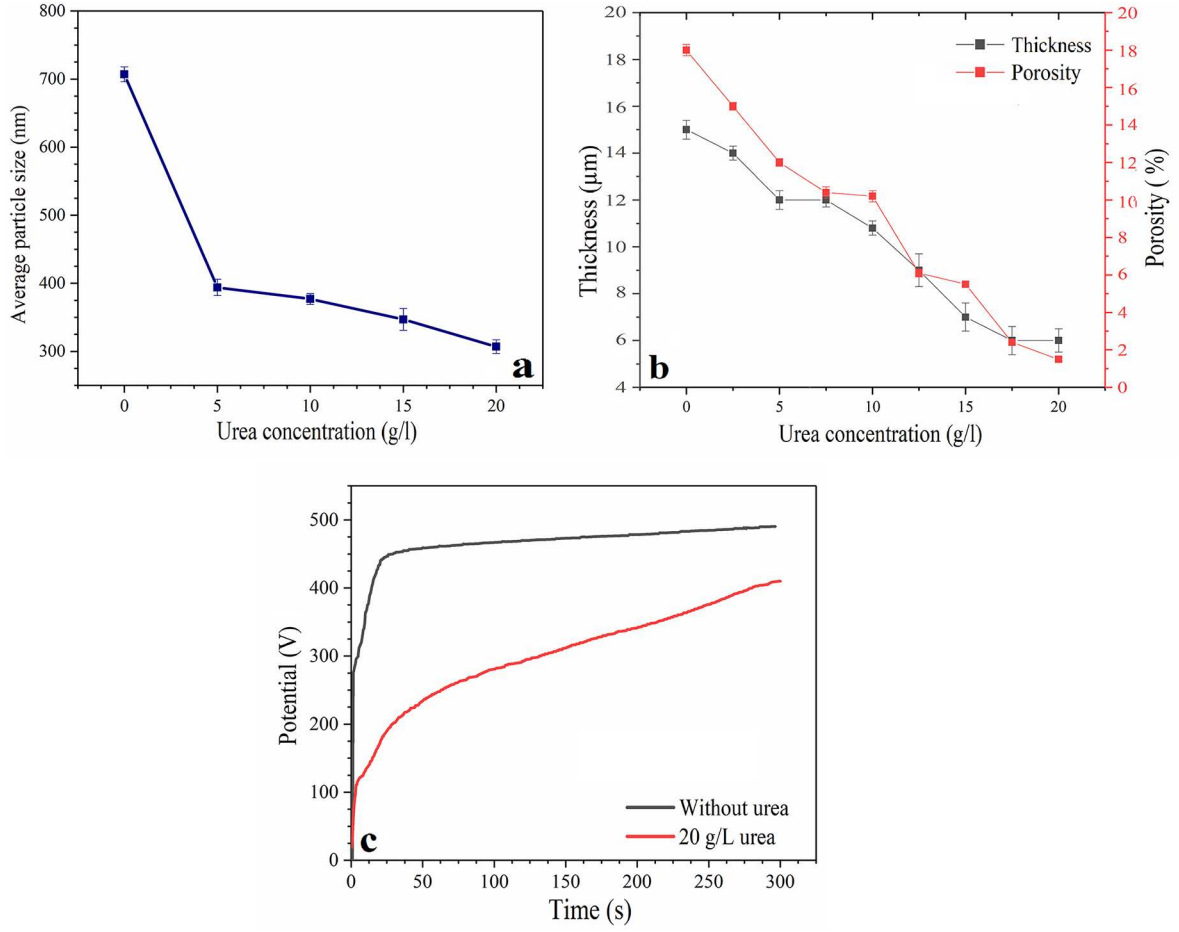

Fig. 9. a) Variation of average size of NPs in the suspension versus urea concentration; b) variation of porosity and thickness of films versus urea concentration, c) potential variation diagram with time for MAO coated samples with/without urea.

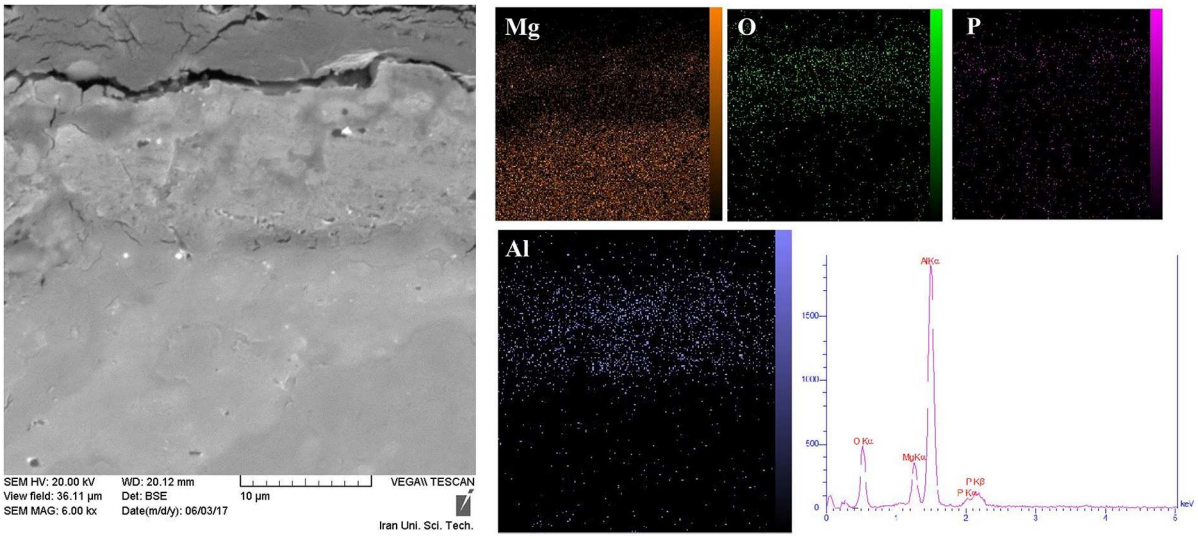

Fig. 10. EDS map of sample with 30 g/l alumina NPs and 20 g/l urea with the current density of 100 mA/cm^2, electrolyte rotation rate of 100 rpm and 5 min duration of PEO coating.

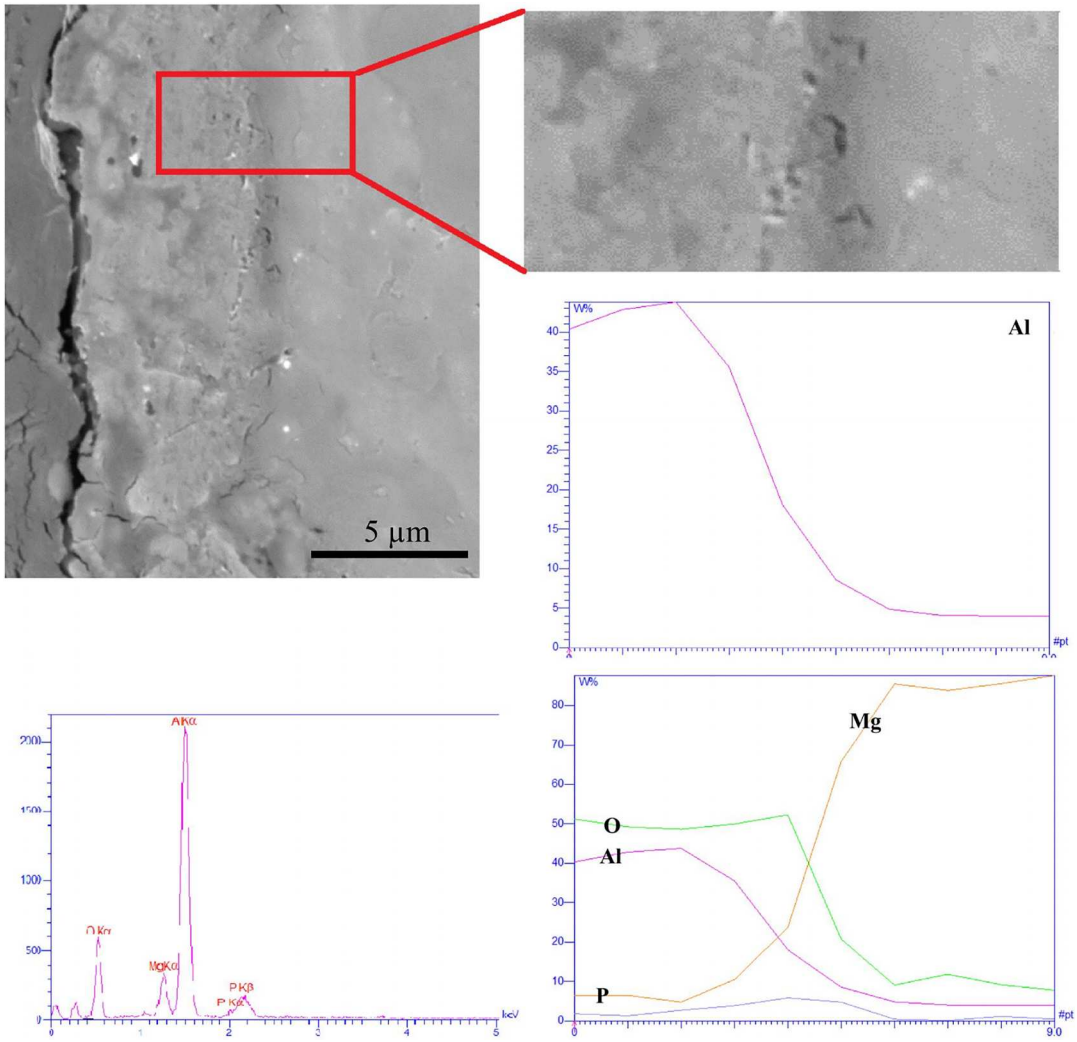

Fig. 11. EDS line of sample with 30 g/l alumina NPs and 20 g/l urea with the current density of 100 mA/cm^2, electrolyte rotation rate of 100 rpm and 5 min duration of PEO coating.

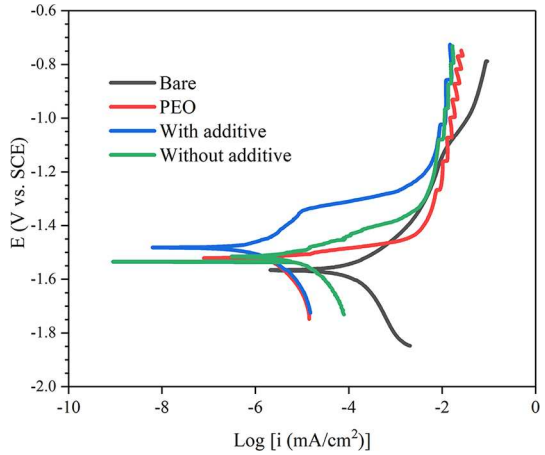

Fig. 12. Polarization curves of Bare, PEO, without additive, and with additive samples with coating condition of 30 g/l alumina NPs in PEO bath and the current density of 100 mA/cm^2, electrolyte rotation rate of 100 rpm and 5 min duration of PEO coating.

produced under different conditions, such as coated in the additive-free electrolyte, NP-free electrolyte and without PEO coatings. Polarization curves of samples coated in electrolytes with (20 g/l) and without urea in the presence of NPs are illustrated in Fig. 12. The results of corrosion resistance, corrosion current density (i_{corr}), and corrosion potential (E_{corr}) were extracted from the polarization curves (through drawing Tafel slopes) [21]. Tafel slopes that were calculated (cathodic slope from −20 mV vs. OCP to −50 mV vs. OCP and anodic slope from +20 mV vs. OCP to +50 mV vs. OCP) are shown in Table 3. The polarization resistance (R_p) is calculated by Stern's Gary's equation (Eqs. (1) and (2)).

$$I_{corr} = \frac{\beta}{Rp} \quad (1)$$

$$\beta = \frac{\beta a \bullet \beta c}{2.3(\beta a + \beta c)} \quad (2)$$

The first noticeable finding was that the coated samples had a higher corrosion resistance than the uncoated samples. Corrosion potential of coated samples was more positive; hence, it stands as a reason for the lower tendency to corrosion [60,61]. It was clear that corrosion current density had been reduced after the addition of NPs to the electrolyte. In the presence of urea, corrosion current density reduction was decreased even further so that corrosion resistance was continuously improved. The oxide film formed on the surface limited the incorporation of corrosive ions and reduced charge transfer in the metal-electrolyte interface. This can be established as the mechanism responsible for the improvement of corrosion resistance. The corrosion resistance of coatings is affected by characteristics of the oxide film including chemical composition, thickness, defects structure and chemical composition of the corrosive medium [62]. With an increase in urea concentration, the incorporation of NPs increases up to a constant level. These NPs reduce the number of possible sites for penetration of corrosive ions into the surface (such as micropores and microcracks). As a result, the corrosion process is hindered over the coating. Filling of micropores due to the incorporation of NPs was also confirmed by SEM images.

Fig. 13 shows the SEM images of samples after the PDP test. The images reveal that the sample with NPs fails less compared to samples without NPs. The sample without coating fails thoroughly following PDP test, and that the surface is covered with corrosion products. The sample with PEO coating failed locally and the coating separated from the substrate since the coating possessed micro-pores and micro-cracks which facilitate the penetration of electrolyte to the coating. The sample with NPs suffered smaller failures than the sample without NPs because filling the micro-pore and micro-crack decreases the number of possible sites for penetration of corrosive ions and the coating. The sample with additive had filled all the preferred locations, which resulted in it being attacked less in comparison to other samples.

The porosity of the coatings was also evaluated using the polarization method. Based on this method, porosity can be evaluated according to the following equation:

$$\text{P. D.} = \frac{Rps}{Rp} \bullet 10^{\left(\frac{\Delta E}{\beta a}\right)}$$

In which R_{ps}, R_p, ΔE, and β_a are the polarization resistance of the substrate without coating, polarization resistance of the coating, the corrosion potential difference between coating and substrate and anodic slope of the substrate, respectively. The results are shown in Table 3. As can be seen, there is good agreement between the results obtained from the software and the polarization method.

3.2.2.2. Electrochemical impedance spectrometry. In order to obtain additional information on the corrosion behavior of samples coated with urea, and to confirm the previous results obtained from PDP, EIS studies were carried out on the samples. To compare corrosion resistance in different types of samples, Nyquist (Fig. 14a) and bode and bode-phase (Fig. 14b and c) plots can be utilized. An Equivalent Electrical Circuit (EEC), as shown in Fig. 14d, was used for the fitting of these data. The parameters obtained from the curves are presented in Table 4. There are two-time constant circuit models in the EEC which represent the dense inner layer in low frequencies and the outer porous layer in high frequencies. In the fitted EEC, R_s is the solution resistance, R_l is the outer porous layer resistance, CPE_l is the constant phase element of the outer porous layer, R_2 is the dense inner layer and CPE_2 is the constant phase element of the dense inner layer. Instead of a pure capacitor, the authors decided to employ a constant phase element due to the non-homogeneity of the surface. Here, the impedance of the constant phase element is described as follows:

$$Z_{CPE} = \frac{1}{T(j\omega)^n} \quad (3)$$

where T is the admittance constant, j represents an imaginary unit, ω is the angular frequency and n is the empirical power of CPE which ranges from 0 to 1. Zero or one show pure resistance or capacitor, respectively. In addition, an inductor loop is considered in low frequencies illustrated in the EEC.

The coating formation mechanism that results in the formation of an outer porous layer and a dense inner layer can also be expressed based

Table 3
Results obtained from potentiodynamic polarization curves of samples deposited with/without urea.

	β_a (mv/decade)	β_c (mV/decade)	i_{corr} (μA/cm^2)	R_p (Ohm·cm^2)	Corrosion rate (mpy)	E (mV vs. SCE)	P/D
Bare	75	64	28	385	25	−1583	6.1
PEO	58	107	6.8	2401	6.2	−1517	3.7
Without additive	78	65	2.8	4172	2.6	−1531	1.6
With additive	113	102	1.5	18,117	1.36	−1482	0.98

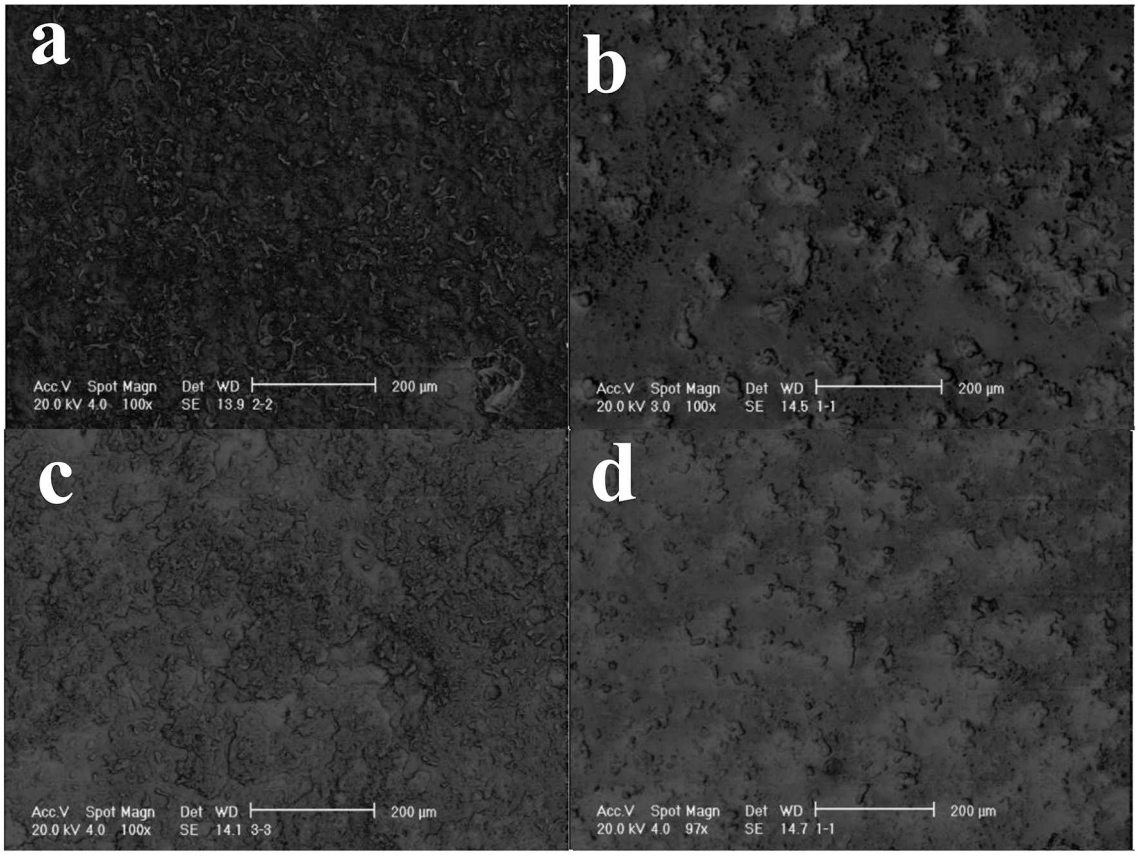

Fig. 13. SEM images of the surfaces after PDP test for the samples, a) bare b) PEO c) without additive d) with additive sample.

on the equivalent circuit used. As mentioned above, the PEO coating consists of an outer porous layer and a barrier layer. This outer porous layer is comprised of electrical discharge channels, cavities, and cracks created during coating formation. Therefore, the equivalent circuit elements used can be attributed to different parts of the coating created. The equivalent circuit used for the different parts of the coating is schematically illustrated in Fig. 14d. Metal dissolution and barrier layer growth occur simultaneously at the start of the PEO process, which can also be observed in the voltage-time curve, the initial step where the voltage is increased linearly. As soon as the surface of the sample is coated with a non-conductive oxide coating, the voltage between the substrate and the electrolyte is rapidly increased, and in a few minutes, the voltage reaches several thousand volts. This voltage is increased to the point where the plasma microscopic discharges cause the coating to break and create a large number of small plasma discharges with a very short life span. These discharges result in local plasma reactions under high temperature and pressure conditions, which results in the formation of a porous outer layer.

The double-layer semi-circle is not observed in Nyquist plots due to its low diameter. The continuity of Nyquist plot below Z′-axis proves the existence of self-induction in the EEC. Based on the EIS results, it can describe the corrosion resistance. As can be observed, there is an induction loop in the magnesium substrate sample and in the PEO coating without the presence of nanoparticles. The existence of this induction loop is due to the kinetic effects of the adsorption-desorption behavior of the intra-electrolyte species such as Cl^- on the metal surface, which is responsible for the corrosion of the electrode surface. It is also seen that with the addition of nanoparticles in the coating bath, and also the addition of urea, this induction loop is no longer seen, indicating that the pitting corrosion of the magnesium surface has disappeared. It can be deduced that the presence of nanoparticles in the coating by filling the cavities of the coating as well as increasing the coating density, prevents the penetration of corrosive ions such as chlorine ions into the substrate, thus preventing the corrosion of the cavities. The largest semi-circle in Nyquist plots belongs to the sample coated in the electrolyte containing urea. No-urea, no-NP and uncoated samples showed smaller semi-circles, respectively. As the diameter of semi-circles represents polarization resistance, it may be concluded that the highest corrosion resistance belongs to the sample with urea [63]. No-urea and no-NP samples stood next in this category. It should be noted that the addition of Al_2O_3 NPs into the electrolyte leads to filling the pores of the oxide layer, and consequently improvement of corrosion resistance. This can be clearly observed by SEM images on the morphology of the samples [64,65]. Slight diversions from the ideal state (chi-square) are shown for n in Table 4. Accordingly, n was increased with the addition of urea and NPs which shows improvement of surface uniformity. The small value of n indicates that there are numerous active sites for the corrosion process.

It can be observed in the bode plot shown in Fig. 14b that the impedance was increased with the addition of urea in low frequencies ($|Z_{0.01\ Hz}|$), therefore enhancing the resistance of the whole film was improved (values are given in Table 4). The highest resistance was observed in the sample with urea. No-urea, no-NP and uncoated samples were once again next in resistance, respectively. This is mainly caused by the incorporation of NPs. In other words, filling of micropores and microcracks resulted in an increase of incorporation of NPs and improvement of the corrosion resistance of the film.

The bode-phase plot is also illustrated in Fig. 14b. There are two time-constants clearly observed in the plot. For coated samples, the first constant appears at approximately high frequencies while the second constant is seen at low frequencies. However, lower phase angles emerged in uncoated samples at a high frequency where aggressive ions were able to pass through the surface layers more conveniently and reach the substrate. Then, the addition of NPs has had a desirable effect.

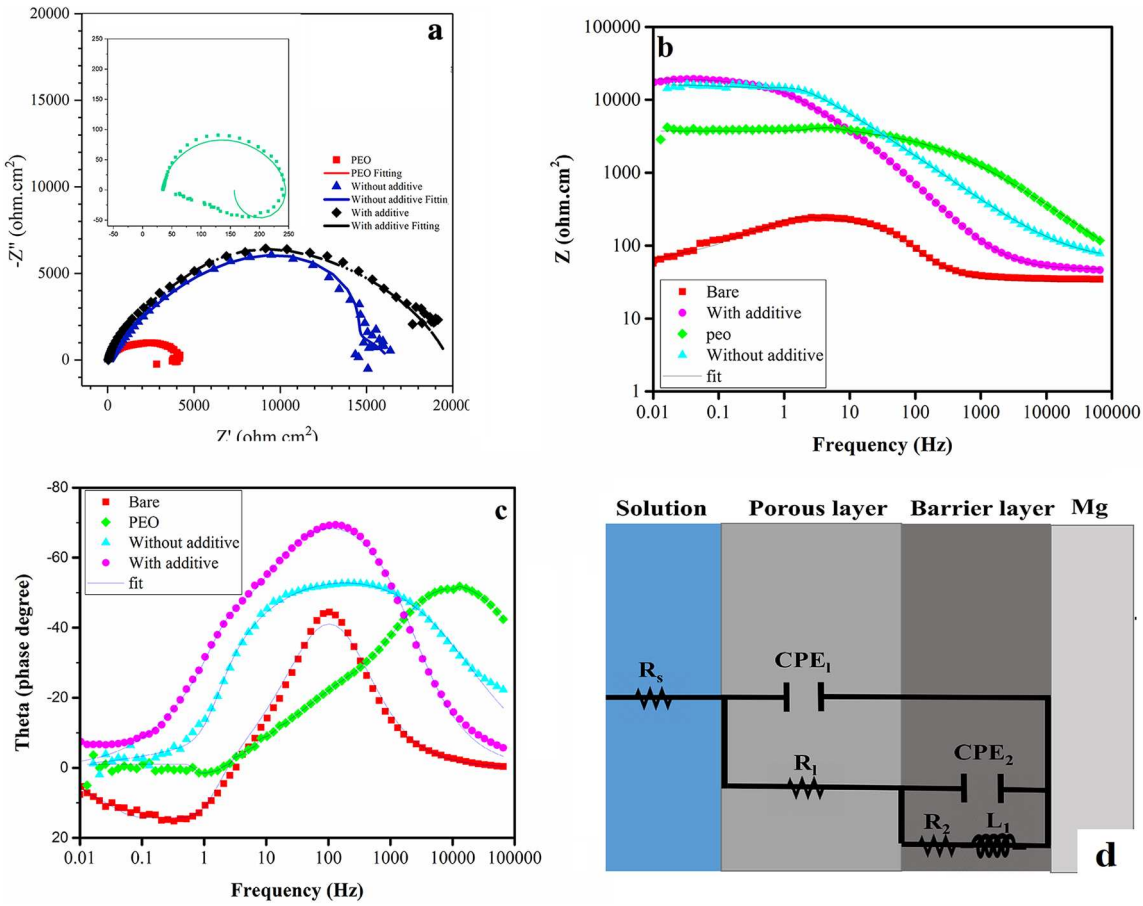

Fig. 14. a) Nyquist plots; b) bode plots and c) bode-phase plots of samples coated with/without urea and c) equivalent circuit to fit the impedance data.

The coated sample which was produced in the presence of urea and NPs reached −70° and had a proper capacitor behavior. In contract, capacitor behavior deteriorated in the sample without urea and phase angle increased which reflects the loss of corrosion resistance. It should be noted that the presence of NPs resulted in an improvement of the corrosion resistance of the oxide film. The broadening of the limited frequency in bode-phase plots implies a better capacitor behavior and a lowered presence of corrosive agents at the surface-coating interface. Improvement of resistance was probably due to an increase in the density of the oxide film or inability of the aggressive ions in attacking the oxide film.

It may be concluded, according to the impedance data, that the highest corrosion resistance belonged to the sample deposited with urea. There were no-urea, no-NP, and uncoated samples afterward. This order is entirely in line with other results obtained from morphology studies and polarization evaluations.

3.2.3. Mechanical behavior

Fig. 15 illustrates the wear results for samples coated under various conditions. Fig. 15a corresponds to the coefficient of friction (COF) of samples. As it can be observed, the COF, in terms of distance, was initially increased for the sample coated in the electrolyte containing urea, and then decreased after 100 m. The COF of the sample coated in the electrolyte without urea was almost constant. However, the sample without NPs maintained an increasing trend with intensive fluctuations after 100 m. As shown in the figure, COF of samples with urea, without urea and without NPs are illustrated from the top to bottom, respectively. Attributing the curve on top for the sample coated in the electrolyte containing urea demonstrated the highest COF due to the presence of the highest amount of alumina NPs. In fact, NPs create a high COF when they contact the pin. The sample without urea was in the middle which was probably due to the presence of a smaller number of alumina NPs in contact with the pin [34].

The continuous increase in COF of the sample coated in the electrolyte containing urea in the first 75 m can be ascribed to the fact that NPs were initially incorporated into the pores and magnesium oxide. After a given amount of time (or distance), NPs were exposed to the pin, increasing COF and reducing wear rate. This was also seen in the SEM image where alumina NPs present in the pores and magnesium oxide. After 100 m, the COF pursued a decreasing trend and fell to 0.45 which is equal to the sample coated in the absence of urea. The general trend of variations indicates that urea was possibly effective in the

Table 4
Fitting results of impedance curves in samples coated with/without urea.

Sample	R_1 (Ohm·cm^2)	CPE_1 (Ω^{-1}·cm^{-2}·S^n) (∗10^{-6})	n_1	R_2 (Ohm·cm^2)	CPE_2 (Ω^{-1}·cm^{-2}·S^n)	n_2	L (H·cm^2)	Chi-squared
Bare	5	7.7E−3	0.1	120	40	0.89	17	0.2
PEO	582	7.50E−05	0.62	3800	9.20	0.6	62	0.027
Without additive	1665	6.40E−05	0.64	14,790	6.02	0.64	665	0.0026
With additive	2364	2.90E−05	0.68	17,376	3.20	0.85	865	0.0027

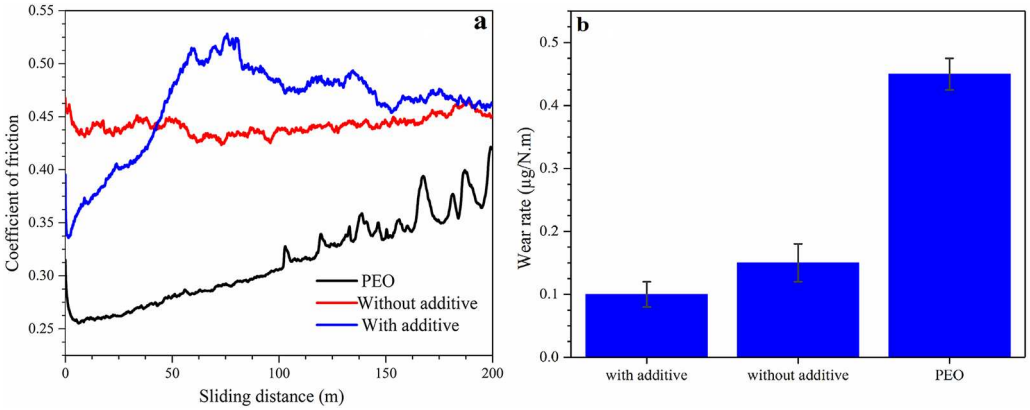

Fig. 15. a) Friction coefficient variations and b) wear rate variations for samples coated with/without urea.

improvement of the incorporation of NPs only onto the external surfaces; while, it did not affect the internal layer [66]. In the sample coated in the electrolyte without urea, NPs existed throughout the coating and increase the COF compared to the no-NP sample. Intense fluctuations observed in COF of the no-NP sample after 100 m was most likely due to coating debris which had been detached and contacted the pin [67]. Wear rate variations versus NPs concentration are shown in Fig. 15b. Accordingly, the least wear rate belongs to the sample coated with urea. Again, no-urea and no-NP samples had the next standings which are in agreement with the amount of the incorporation of NPs. It may be concluded that the wear rate was decreased with an increase in the incorporation of NPs [68,69]. The sample coated in presence of urea had a slower wear rate than that of the no-NP sample which was due to filling of pores existent on surface of the porous PEO coating [17,70].

SEM images of the specimens after the wear test are shown in Fig. 16. As can be observed, the presence of alumina NPs in the coating has a positive effect on the wear behavior of the coating. Fig. 16 shows the worn surface of samples that coated at various conditions such as coating without NPs, with NPs and with adding urea. Fig. 16 indicates that the coating with low incorporated alumina NPs is fully worn after the wear test and even reaches the magnesium alloy substrate. Unlike the specimen with a lower amount of incorporated alumina NPs (sample with NPs and without additive), the initial failure is not observed in the coating containing high incorporated alumina NPs (sample with NP and additive). Samples with high incorporation of alumina NPs have abrasive wear mechanism (samples coating with additive). In the case of samples with low incorporation of alumina NPs, the dominant wear mechanism is adhesive wear (samples coated without additive). The dominant wear mechanism for other samples is a mixture of abrasive and adhesive wear.

As the SEM images suggest, by adding the NPs to the coating, the faults in the coating such as porosity are reduced, resulting in an improved wear rate and wear behavior of coatings [66]. The SEM images of NP-free specimens show that the pores have been reduced by adding the NPs. Yu et al. [71] have reported these poor areas in their studies and stated that these areas result in cracking, crushing, and pouring of the coating over the wear process. Their research reveals that by increasing the hardness of the surface, the wear resistance is enhanced [17,72,73]. This situation is improved even further by adding alumina NPs. These results are consistent with those of other researchers in increasing the hardness of NPs [33,34]. Generally, it is believed that the type of wear in PEO coating is abrasive wear, and with the incorporation of hard NPs, it is therefore changed to abrasive wear.

Hardness test was conducted on all the samples. For this purpose, the test was repeated 5 times on each individual specimen and the average value of the measurement is reported. Results show that applying PEO coating hardness increased by > 5.5 times (from 50.9 to 280.7). With the addition of Alumina NPs to coating, hardness increased significantly up to 15 times than the hardness of the substrate (from 50.9 to 777.4). By adding the additive, hardness was noticeably improved (from 777.4 to 850.7). Owing to the PEO coating is the ceramic coating, the hardness was improved in the first stage. In the second stage, the increase of hardness is due to the addition of hard Alumina NPs, which resulted in an increase in the average hardness [26].

4. Conclusion

The effects of different additives and particle size on the incorporation of alumina particles inside the coating and properties of the nanocomposite PEO films coated on AZ31B magnesium alloy substrates were investigated. The highest incorporation of particles was acquired with the application of urea and using NPs. The optimum urea concentration was 20 g/l which lead to the highest incorporated amount of NPs due to their excellent dispersion in the electrolyte, and also by preventing agglomeration. Dispersion caused the presence of smaller particles resulting in improvement of the incorporation process. The highest incorporated amount of NPs and the consequent reduction of

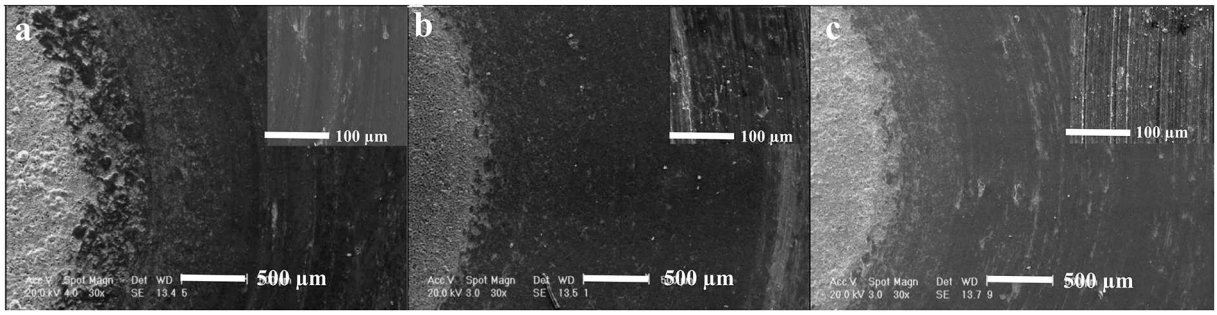

Fig. 16. SEM images of worn surfaces a) PEO b) without additive c) with additive sample.

porosity in the sample coated in the suspension containing 20 g/l of urea resulted in the highest corrosion resistance. In addition, wear behavior studies indicated that the lowest wear rate also belongs to the sample coated in the electrolyte containing 20 g/l of urea.

Author contribution statement

M. Asgari: Methodology, Validation, Investigation, Writing - Original Draft

M. Aliofkhazraei: Conceptualization, Methodology, Resources, Writing - Review & Editing, Supervision

Gh. Barati Darband: Validation, Writing - Original Draft

A. Sabour Rouhaghdam: Supervision

Declaration of competing interest

The authors declare that they have no known competing financial interests or personal relationships that could have appeared to influence the work reported in this paper.

References

[1] G.-L. Song, Corrosion of Magnesium Alloys, Elsevier, 9781845697082, 2011.
[2] G.L. Song, A. Atrens, Corrosion mechanisms of magnesium alloys, Adv. Eng. Mater. 1 (1999) 11–33.
[3] M. Esmaily, J. Svensson, S. Fajardo, N. Birbilis, G. Frankel, S. Virtanen, R. Arrabal, S. Thomas, L. Johansson, Fundamentals and advances in magnesium alloy corrosion, Prog. Mater. Sci. 89 (2017) 92–193.
[4] Z.A.X.Y.Q. Yufeng, W.Z.H.Y.C. Ying, Chemical surface treatment for magnesium alloys [J], Corrosion & Protection 2 (2000) 002.
[5] G. Song, A. Atrens, Understanding magnesium corrosion—a framework for improved alloy performance, Adv. Eng. Mater. 5 (2003) 837–858.
[6] Z. Shi, A. Atrens, An innovative specimen configuration for the study of Mg corrosion, Corros. Sci. 53 (2011) 226–246.
[7] G. Song, A. Atrens, D. St John, X. Wu, J. Nairn, The anodic dissolution of magnesium in chloride and sulphate solutions, Corros. Sci. 39 (1997) 1981–2004.
[8] G. Song, A. Atrens, D. Stjohn, J. Nairn, Y. Li, The electrochemical corrosion of pure magnesium in 1 N NaCl, Corros. Sci. 39 (1997) 855–875.
[9] S. Gnedenkov, S. Sinebryukhov, V. Egorkin, I. Vyalyi, D. Mashtalyar, K. Nadaraia, D. Ryabov, V. Buznik, Formation and properties of composite coatings on aluminum alloys, Russ. J. Inorg. Chem. 62 (2017) 1–11.
[10] A. Yerokhin, X. Nie, A. Leyland, A. Matthews, S. Dowey, Plasma electrolysis for surface engineering, Surf. Coat. Technol. 122 (1999) 73–93.
[11] G. Barati Darband, M. Aliofkhazraei, P. Hamghalam, N. Valizade, Plasma electrolytic oxidation of magnesium and its alloys: mechanism, properties and applications, Journal of Magnesium and Alloys 5 (2017) 74–132.
[12] M. Aliofkhazraei, A.S. Rouhaghdam, P. Gupta, Nano-fabrication by cathodic plasma electrolysis, Critical Reviews in Solid State and Materials Sciences 36 (2011) 174–190.
[13] M. Aliofkhazraei, R.S. Gharabagh, M. Teimouri, M. Ahmadzadeh, G.B. Darband, H. Hasannejad, Ceria embedded nanocomposite coating fabricated by plasma electrolytic oxidation on titanium, J. Alloys Compd. 685 (2016) 376–383.
[14] M. Aliofkhazraei, A.S. Rouhaghdam, Wear and coating removal mechanism of alumina/titania nanocomposite layer fabricated by plasma electrolysis, Surf. Coat. Technol. 205 (2011) S57–S62.
[15] F. Einkhah, K.M. Lee, M.A.F. Sani, B. Yoo, D.H. Shin, Structure and corrosion behavior of oxide layer with Zr compounds on AZ31 Mg alloy processed by two-step plasma electrolytic oxidation, Surf. Coat. Technol. 238 (2014) 75–79.
[16] S.V. Gnedenkov, S.L. Sinebryukhov, D.V. Mashtalyar, I.M. Imshinetskiy, Electrochemical and mechanical properties of composite coatings obtained on MA8 alloy in disperse electrolytes with ZrO_2 and SiO_2 nanoparticles, Tsvetnye Metally 2015 (2015) 60–65.
[17] S. Gnedenkov, S. Sinebryukhov, D. Mashtalyar, I. Imshinetskiy, A. Samokhin, Y.V. Tsvetkov, Fabrication of coatings on the surface of magnesium alloy by plasma electrolytic oxidation using ZrO_2 and SiO_2 nanoparticles, J. Nanomater. 16 (2015) 196.
[18] F. Vaz, L. Rebouta, Superhard Nanocomposite Ti-Si-N Coatings, (2002), pp. 143–149.
[19] S. Zhang, D. Sun, Y. Fu, H. Du, Recent advances of superhard nanocomposite coatings: a review, Surf. Coat. Technol. 167 (2003) 113–119.
[20] S.V. Gnedenkov, S.L. Sinebryukhov, D.V. Mashtalyar, I.M. Imshinetskiy, A.V. Samokhin, Y.V. Tsvetkov, Fabrication of coatings on the surface of magnesium alloy by plasma electrolytic oxidation using ZrO < inf > 2 < /inf > and SiO < inf > 2 < /inf > nanoparticles, J. Nanomater. 2015 (2015).
[21] M. Gheytani, M. Aliofkhazraei, H. Bagheri, H. Masiha, A.S. Rouhaghdam, Wettability and corrosion of alumina embedded nanocomposite MAO coating on nanocrystalline AZ31B magnesium alloy, J. Alloys Compd. 649 (2015) 666–673.
[22] Effects of Al_2O_3 nano-additive on performance of micro-arc oxidation coatings formed on AZ91D Mg alloy, Material Science 30 (2014) 984–990.
[23] S. Sarbishei, M.A.F. Sani, M.R. Mohammadi, Effects of alumina nanoparticles concentration on microstructure and corrosion behavior of coatings formed on titanium substrate via PEO process, Ceram. Int. 42 (2016) 8789–8797.
[24] M. Gheytani, H.R. Bagheri, H.R. Masiha, M. Aliofkhazraei, A. Sabour Rouhaghdam, T. Shahrabi, Effect of SMAT preprocessing on MAO fabricated nanocomposite coating, Surf. Eng. 30 (2014) 244–255.
[25] S.-C. Yeh, D.-S. Tsai, S.-Y. Guan, C.-C. Chou, Influences of urea and sodium nitrite on surface coating of plasma electrolytic oxidation, Appl. Surf. Sci. 356 (2015) 135–141.
[26] Y.K. Pan, C.Z. Chen, D.G. Wang, X. Yu, Z.Q. Lin, Influence of additives on microstructure and property of microarc oxidized Mg-Si-O coatings, Ceram. Int. 38 (2012) 5527–5533.
[27] M. Vasilyeva, V. Rudnev, I. Korotenko, P. Nedozorov, Producing and studying oxide coatings containing manganese and nickel compounds on titanium from electrolyte suspensions, Protection of Metals and Physical Chemistry of Surfaces 48 (2012) 106–115.
[28] S. Sarbishei, M.A.F. Sani, M.R. Mohammadi, Study plasma electrolytic oxidation process and characterization of coatings formed in an alumina nanoparticle suspension, Vacuum 108 (2014) 12–19.
[29] X.-M. Li, Y. Han, Porous nanocrystalline Ti(CxN1 − x) thick films by plasma electrolytic carbonitriding, Electrochem. Commun. 8 (2006) 267–272.
[30] X.-M. Li, Y. Han, Y.-S. Li, Synthesis of nanocrystallineTi (CxN1 − x) thick films on titanium by plasma electrolytic carbonitriding, Surf. Coat. Technol. 201 (2007) 5326–5329.
[31] D.-Y. Kim, M. Kim, H.-E. Kim, Y.-H. Koh, H.-W. Kim, J.-H. Jang, Formation of hydroxyapatite within porous TiO_2 layer by micro-arc oxidation coupled with electrophoretic deposition, Acta Biomater. 5 (2009) 2196–2205.
[32] M. Mu, J. Liang, X. Zhou, Q. Xiao, One-step preparation of TiO2/MoS2 composite coating on Ti6Al4V alloy by plasma electrolytic oxidation and its tribological properties, Surf. Coat. Technol. 214 (2013) 124–130.
[33] H. Sharifi, M. Aliofkhazraei, G.B. Darband, A.S. Rouhaghdam, Characterization of PEO nanocomposite coatings on titanium formed in electrolyte containing atenolol, Surf. Coat. Technol. 304 (2016) 438–449.
[34] H. Sharifi, M. Aliofkhazraei, G.B. Darband, A.S. Rouhaghdam, Tribological properties of PEO nanocomposite coatings on titanium formed in electrolyte containing ketoconazole, Tribol. Int. 102 (2016) 463–471.
[35] C. Blawert, S.P. Sah, J. Liang, Y. Huang, D. Höche, Role of sintering and clay particle additions on coating formation during PEO processing of AM50 magnesium alloy, Surf. Coat. Technol. 213 (2012) 48–58.
[36] X. Lu, C. Blawert, Y. Huang, H. Ovri, M.L. Zheludkevich, K.U. Kainer, Plasma electrolytic oxidation coatings on Mg alloy with addition of SiO_2 particles, Electrochim. Acta 187 (2016) 20–33.
[37] W. Yeung, I. Sukhorukova, D. Shtansky, E. Levashov, I. Zhitnyak, N. Gloushankova, P.V. Kiryukhantsev-Korneev, M. Petrzhik, A. Matthews, A. Yerokhin, Characteristics and in vitro response of thin hydroxyapatite–titania films produced by plasma electrolytic oxidation of Ti alloys in electrolytes with particle additions, RSC Adv. 6 (2016) 12688–12698.
[38] L. Wang, W. Fu, L. Chen, Preparation of ZrO_2 coatings by plasma electrolytic oxidation on surface of magnesium alloys and its discharge characteristics, Kuei Suan Jen Hsueh Pao, J. Chin. Ceram. Soc. 40 (2012) 1802–1806.
[39] M. Mohedano, C. Blawert, M.L. Zheludkevich, Silicate-based Plasma Electrolytic Oxidation (PEO) coatings with incorporated CeO < inf > 2 < /inf > particles on AM50 magnesium alloy, Mater. Des. 86 (2015) 735–744.
[40] M. Asgari, M. Aliofkhazraei, G.B. Darband, A.S. Rouhaghdam, Evaluation of alumina nanoparticles concentration and stirring rate on wear and corrosion behavior of nanocomposite PEO coating on AZ31 magnesium alloy, Surf. Coat. Technol. 309 (2017) 124–135.
[41] T.S. Lim, H.S. Ryu, S.H. Hong, Electrochemical corrosion properties of CeO_2-containing coatings on AZ31 magnesium alloys prepared by plasma electrolytic oxidation, Corros. Sci. 62 (2012) 104–111.
[42] S. Di, Y. Guo, H. Lv, J. Yu, Z. Li, Microstructure and properties of rare earth CeO_2-doped TiO_2 nanostructured composite coatings through micro-arc oxidation, Ceram. Int. 41 (2015) 6178–6186.
[43] X. Lu, M. Mohedano, C. Blawert, E. Matykina, R. Arrabal, K.U. Kainer, M.L. Zheludkevich, Plasma electrolytic oxidation coatings with particle additions–a review, Surf. Coat. Technol. 307 (2016) 1165–1182.
[44] F.H. Cao, J.L. Cao, Z. Zhang, J.Q. Zhang, C.N. Cao, Plasma electrolytic oxidation of AZ91D magnesium alloy with different additives and its corrosion behavior, Mater. Corros. 58 (2007) 696–703.
[45] M. Aliofkhazraei, A.S. Rouhaghdam, Study of nanoparticle adsorption in single discharge of plasma electrolysis, Electrochem. Commun. 20 (2012) 88–91.
[46] S. Mirzamohammadi, H. Khorsand, M. Aliofkhazraei, Effect of different organic solvents on electrodeposition and wear behavior of Ni-alumina nanocomposite coatings, Surf. Coat. Technol. 313 (2017) 202–213.
[47] D. Thiemig, A. Bund, Influence of ethanol on the electrocodeposition of Ni/Al_2O_3 nanocomposite films, Appl. Surf. Sci. 255 (2009) 4164–4170.
[48] H. Gül, F. Kılıç, M. Uysal, S. Aslan, A. Alp, H. Akbulut, Effect of particle concentration on the structure and tribological properties of submicron particle SiC reinforced Ni metal matrix composite (MMC) coatings produced by electrodeposition, Appl. Surf. Sci. 258 (2012) 4260–4267.
[49] X. Zhang, J. Qin, M.K. Das, R. Hao, H. Zhong, A. Thueploy, S. Limpanart, Y. Boonyongmaneerat, M. Ma, R. Liu, Co-electrodeposition of hard Ni-W/diamond nanocomposite coatings, Sci. Rep. 6 (2016).
[50] M.-D. Ger, B.J. Hwang, Effect of surfactants on codeposition of PTFE particles with electroless Ni-P coating, Mater. Chem. Phys. 76 (2002) 38–45.
[51] J. Guo, L. Wang, S. Wang, J. Liang, Q. Xue, F. Yan, Preparation and performance of

a novel multifunctional plasma electrolytic oxidation composite coating formed on magnesium alloy, J. Mater. Sci. 44 (2009) 1998.
[52] D. Sreekanth, N. Rameshbabu, K. Venkateswarlu, Effect of various additives on morphology and corrosion behavior of ceramic coatings developed on AZ31 magnesium alloy by plasma electrolytic oxidation, Ceram. Int. 38 (2012) 4607–4615.
[53] C. Fong, D. Wells, I. Krodkiewska, P.G. Hartley, C.J. Drummond, New role for urea as a surfactant headgroup promoting self-assembly in water, Chem. Mater. 18 (2006) 594–597.
[54] D. Wells, C. Fong, I. Krodkiewska, C.J. Drummond, Nonionic urea surfactants: influence of hydrocarbon chain length and positional isomerism on the thermotropic and lyotropic phase behavior, J. Phys. Chem. B 110 (2006) 5112–5119.
[55] V. Dehnavi, D.W. Shoesmith, B.L. Luan, M. Yari, X.Y. Liu, S. Rohani, Corrosion properties of plasma electrolytic oxidation coatings on an aluminium alloy - the effect of the PEO process stage, Mater. Chem. Phys. 161 (2015) 49–58.
[56] V. Dehnavi, B.L. Luan, X.Y. Liu, D.W. Shoesmith, S. Rohani, Correlation between plasma electrolytic oxidation treatment stages and coating microstructure on aluminum under unipolar pulsed DC mode, Surf. Coat. Technol. 269 (2015) 91–99.
[57] A. Yerokhin, L. Snizhko, N. Gurevina, A. Leyland, A. Pilkington, A. Matthews, Discharge characterization in plasma electrolytic oxidation of aluminium, J. Phys. D. Appl. Phys. 36 (2003) 2110.
[58] F. Xu, Y. Xia, G. Li, The mechanism of PEO process on Al–Si alloys with the bulk primary silicon, Appl. Surf. Sci. 255 (2009) 9531–9538.
[59] Y. Guan, Y. Xia, G. Li, Growth mechanism and corrosion behavior of ceramic coatings on aluminum produced by autocontrol AC pulse PEO, Surf. Coat. Technol. 202 (2008) 4602–4612.
[60] Z. Cui, Z. Shao, Z. Liu, L. Zhao, Y. Tian, Effects of additives on properties of ceramic coatings formed by micro-arc oxidation on AZ91D Mg alloy, Cailiao Yanjiu Xuebao/Chinese Journal of Materials Research 23 (2009) 193–198.
[61] F. Liu, D. Shan, Y. Song, E.H. Han, Effect of additives on the properties of plasma electrolytic oxidation coatings formed on AM50 magnesium alloy in electrolytes containing K2ZrF6, Surf. Coat. Technol. 206 (2011) 455–463.
[62] D. Sreekanth, N. Rameshbabu, K. Venkateswarlu, C. Subrahmanyam, L. Rama Krishna, K. Prasad Rao, Effect of K2TiF6 and Na2B4O7 as electrolyte additives on pore morphology and corrosion properties of plasma electrolytic oxidation coatings on ZM21 magnesium alloy, Surf. Coat. Technol. 222 (2013) 31–37.
[63] O. Mokhnachuk, S. Soloviev, A.Y. Kapran, Effect of rare-earth element oxides (La_2O_3, Ce_2O_3) on the structural and physico-chemical characteristics of Pd/Al_2O_3 monolithic catalysts of nitrogen oxide reduction by methane, Catal. Today 119 (2007) 145–151.
[64] Y. Ma, N. Liu, Y. Wang, J. Wang, H. Guo, Effect of chromate additive on corrosion resistance of MAO coatings on magnesium alloys, Kuei Suan Jen Hsueh Pao/Journal of the Chinese Ceramic Society 39 (2011) 1493–1497.
[65] A. Ghasemi, V.S. Raja, C. Blawert, W. Dietzel, K.U. Kainer, Study of the structure and corrosion behavior of PEO coatings on AM50 magnesium alloy by electrochemical impedance spectroscopy, Surf. Coat. Technol. 202 (2008) 3513–3518.
[66] Y. Wang, B. Jiang, L. Guo, T. Lei, Tribological behavior of microarc oxidation coatings formed on titanium alloys against steel in dry and solid lubrication sliding, Appl. Surf. Sci. 252 (2006) 2989–2998.
[67] Z. Mahidashti, M. Aliofkhazraei, N. Lotfi, Review of nickel-based electrodeposited tribo-coatings, Trans. Indian Inst. Metals 71 (2) (2018) 257–295, https://doi.org/10.1007/s12666-017-1175-x.
[68] L.R. Krishna, A.S. Purnima, G. Sundararajan, A comparative study of tribological behavior of microarc oxidation and hard-anodized coatings, Wear 261 (2006) 1095–1101.
[69] S.-m. Li, X.-m. Yu, J.-h. Liu, M. Yu, L. Wu, K. Yang, Microstructure and abrasive wear behaviour of anodizing composite films containing SiC nanoparticles on Ti6Al4V alloy, J. Cent. South Univ. 21 (2014) 4415–4423.
[70] H. Li, Y. Sun, J. Zhang, Effect of ZrO_2 particle on the performance of micro-arc oxidation coatings on Ti_6Al_4V, Appl. Surf. Sci. 342 (2015) 183–190.
[71] L. Yu, J. Cao, Y. Cheng, An improvement of the wear and corrosion resistances of AZ31 magnesium alloy by plasma electrolytic oxidation in a silicate–hexametaphosphate electrolyte with the suspension of SiC nanoparticles, Surf. Coat. Technol. 276 (2015) 266–278.
[72] S.V. Gnedenkov, Y.P. Sharkeev, S.L. Sinebryukhov, O.A. Khrisanfova, E.V. Legostaeva, A.G. Zavidnaya, A.V. Puz, I.A. Khlusov, D.P. Opra, Functional coatings formed on the titanium and magnesium alloys as implant materials by plasma electrolytic oxidation technology: fundamental principles and synthesis conditions, Corros. Rev. 34 (2016) 65–83.
[73] S. Gnedenkov, S. Sinebryukhov, D. Mashtalyar, I. Imshinetskiy, A. Gnedenkov, A. Samokhin, Y. Tsvetkov, Protective composite coatings obtained by plasma electrolytic oxidation on magnesium alloy MA8, Vacuum 120 (2015) 107–114.